Ab initio analysis of proton transfer dynamics in $(H_2O)_3H^+$

Phillip L. Geissler, Christoph Dellago *, and David Chandler †
Department of Chemistry, University of California, Berkeley, CA 94720

Jürg Hutter and Michele Parrinello
Max-Planck-Institut für Festkörperforschung, Heisenbergstr, 1, 70569 Stuttgart, Germany

We have harvested *ab initio* trajectories of proton transfer in $(H_2O)_3H^+$ by combining Car-Parrinello molecular dynamics (CPMD) with the transition path sampling method. Two transition state regions contribute to these dynamics, with saddle points similar to those identified by Geissler, Dellago, and Chandler for an empirical model of the same cluster [*Phys. Chem. Chem. Phys.* **1**, 1317]. As in that model, the location of a transition state along a finite-temperature trajectory indicates that proton transfer is driven by reorganization of the oxygen ring. From vibrational properties it is estimated that the characteristic time for proton transfer is ~ 1 ns at a temperature of 300 K.

1. Introduction

Simulating the dynamics of chemical transformations poses a significant challenge when reaction coordinates are unknown. At the heart of this challenge lie the long time scales associated with activated events and the computational difficulty of evaluating nuclear forces accurately. The former problem may in principle be overcome using an importance sampling in trajectory space, as prescribed by the method of transition path sampling[1–3]. The latter problem is severe when electronic structure calculations are required at each discrete time step in order to integrate nuclear equations of motion. Accurate quantum chemistry calculations are uniformly too expensive for this purpose for more than a few degrees of freedom. The most efficient *ab initio* alternative for computing forces is provided by density functional theory (DFT). Although DFT is inherently inexact when empirically designed functionals are used, well-parameterized functionals such as BLYP give accurate results for many chemically interesting applications[4–6]. By combining path sampling with dynamics generated by DFT, one should in principle be able to study the microscopic mechanisms of chemical reactions efficiently.

In this letter we demonstrate that sampling reactive trajectories computed by DFT-based Car-Parrinello molecular dynamics (CPMD) is indeed feasible. In particular, we have harvested proton transfer trajectories for the protonated water trimer, $(H_2O)_3H^+$. In order to perform this sampling efficiently, it is necessary to treat the degrees of freedom associated with the Kohn-Sham wavefunction specially, as discussed in Section II. The trajectories we collect, also described in Section II, qualitatively resemble those generated by an empirical model of this cluster[7]. In addition we have located a member of the transition state ensemble using a separatrix analysis. This analysis is presented in Section III. In distinguishing the transition state from nearby configurations, we find that rearrangement of the oxygen ring plays a dominant role in proton transfer dynamics. In Section IV we use transition state theory to estimate the rate of proton transfer at room temperature.

2. Harvesting CPMD trajectories

The transition path sampling method achieves an importance sampling of reactive pathways by requiring that newly generated trajectories satisfy appropriate boundary conditions. Specifi-

*Current address: Department of Chemistry, University of Rochester, Rochester, NY 14627
†Author to whom correspondence should be addressed. Electronic address: chandler@cchem.berkeley.edu.

cally, a path is rejected unless it begins in the reactant basin of attraction, A, and visits the product basin of attraction, B, at some point along the trajectory. It is therefore necessary for efficient sampling that a trial trajectory satisfy these boundary conditions with reasonable probability. ($\sim 40\%$ is optimal.[8]) In successful applications of the method, new trajectories have been generated using "shooting" moves. In these moves, momenta at a certain time along an old trajectory are displaced by a small, randomly chosen amount, and equations of motion are integrated to the endpoints of the new trajectory. Provided the computed dynamics of the system are nearly reversible, this algorithm produces a trial path which is arbitrarily similar to the initial path. A desired acceptance probability, $p_{\rm acc}$, may in principle be obtained simply by tuning the magnitude of the momentum displacement.

When using density functional theory to study nuclear dynamics on the Born-Oppenheimer surface, care must be taken to preserve the inherent reversibility of the motion. In many applications, forces are computed by numerically seeking the electron density which minimizes the energy functional, $E[\{\psi_i\},\{R_I\}]$, at each time step. $\{\psi_i\}$ and $\{R_I\}$ denote the occupied single-particle Kohn-Sham orbitals and the nuclear positions, respectively. While this method gives forces which are in principle correct, the dynamics it generates are not rigorously reversible when the initial conditions for optimization are taken from a previous time step and the optimization accuracy is finite. The degree of reversibility may be improved by increasing the accuracy of this search, but the process is costly, and an efficient alternative exists. The molecular dynamics method of Car and Parrinello[9] avoids a separate minimization at each time step by instead propagating the electron density according to a reversible, though fictitious, dynamics. In doing so, the time derivatives of the Kohn-Sham orbitals, $\{\dot{\psi}_i\}$, are introduced as additional degrees of freedom in the equations of motion. Although a price is paid in the length of a time step which produces stable dynamics near the Born-Oppenheimer surface, the gain in reversibility makes CPMD a more suitable choice for the purposes of path sampling.

To perform a shooting move, we select a time step from an existing CPMD trajectory and displace only the nuclear momenta, leaving the $\{\dot{\psi}_i\}$ unchanged. Using the nuclear configuration and Kohn-Sham wavefunction at that time step, the new nuclear momenta, and the unperturbed $\{\dot{\psi}_i\}$, a trial trajectory is computed. The path is then accepted or rejected in the usual manner, according to boundary conditions and criteria appropriate to the desired ensemble of initial conditions. In this scheme the wavefunction $\{\psi_i\}$ and its rate of change $\{\dot{\psi}_i\}$ must be stored from a previous path in order to generate a new one. With current computational resources, it is impractical to store this amount of data at regular intervals along a trajectory. Instead, we select the time steps for the next n shooting moves prior to calculating a trajectory. The corresponding data are stored only at those n time steps. If all n moves are sequentially rejected (an event of probability $(1-p_{\rm acc})^n$ for uncorrelated statistics), the subsequent sequence of n moves is selected and the old trajectory is regenerated, again storing data only at the desired time steps. For the current work we have used $n = 5$ so that the need to regenerate paths is infrequent. It is also noteworthy that the process of displacing nuclear momenta without changing the $\{\dot{\psi}_i\}$ encourages exchange of energy between nuclei and electrons. In other words, the system is gradually heated away from the Born-Oppenheimer surface. In the simulations we report here, the fictitious kinetic energy arising from the wavefunction dynamics increased on the order of 1% per shooting move. For long path sampling simulations it would be necessary to thermalize the electronic degrees of freedom.

Using the techniques described above, we have performed 25 shooting moves to study proton transfer in $(H_2O)_3H^+$. A standard parameterization of CPMD for aqueous systems was adopted in this work. For all calculations we used the BLYP functional[10], a fictitious mass associated with the $\{\dot{\psi}_i\}$ of 900 amu, a time step of 0.145 fs, cluster boundary conditions [11], a plane wave cutoff of 70 Ry, and a hydrogen mass of 2 amu. For sampling of transition paths, we used an energy consistent with an average temperature of 300 K in the stable state. We characterize the

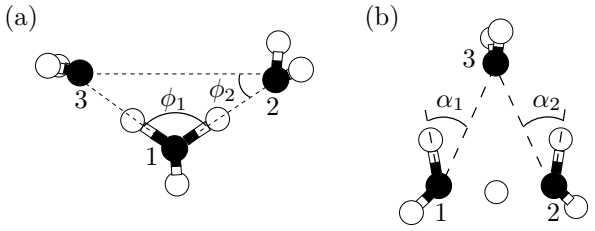

Figure 1. Stable state (a) and lowest energy transition state (b) for proton transfer from molecule 1 to molecule 2. We use the differences between oxygen ring angles, $\Delta\phi = \phi_2 - \phi_1$, and between hydrogen bond angles, $\Delta\alpha = \alpha_1 - \alpha_2$, as order parameters for this process.

stable states by the geometry of the oxygen ring. In terms of angles ϕ_1 and ϕ_2 at the base of this triangle of oxygen atoms, state A is defined by $\Delta\phi \equiv \phi_2 - \phi_1 < -5°$ and state B by $\Delta\phi > 5°$. (See Fig. 1 for a graphical definition of these parameters.)

For proper sampling of transition states, the length of trajectories in the path ensemble, τ, should exceed the time required for the system to commit to a stable basin of attraction, τ_c. For $\tau < \tau_c$ a constraint is effectively imposed in trajectory space, and harvested pathways are not representative of the correct transition path ensemble. In our studies of the Stillinger-David model of this cluster, trajectories initiated in the transition state region recrossed this region with very low probability for times longer than 50 fs[7]. In other words, nearly all trajectories commit to a particular stable state within $\tau_c \approx 50$ fs. In the current work we consider trajectories of length $\tau = 60$ fs.

The initial path for our sampling was constructed by exciting the unstable mode of a transition state configuration. The transition states for proton transfer are known approximately from our studies using the empirical Stillinger-David force field[7] and have also been identified by Wales using DFT[12]. Our sampling of trajectories in the Stillinger-David model revealed two important transition state regions. In both of the corresponding saddle point configurations, the donating and accepting water molecules are related by a symmetry operation. Using CPMD, we have determined these transition state structures more accurately. The lower energy saddle point is shown together with the potential energy minimum configuration in Fig. 1. The transition state depicted in Fig. 1 (b), lying 5.7 kcal/mol above the energy minimum, was used to generate our initial proton transfer pathway. In this C_2-symmetric configuration dipoles of the donating and accepting molecules are aligned antiparallel to one another. The second transition state has C_s symmetry in which these dipoles are roughly parallel and lies approximately 0.7 kcal/mol higher in energy than the first transition state. Our sampling was not thorough enough to observe transitions through the higher energy transition state. Both saddle point configurations were identified by allowing the cluster to relax subject to a constraint of symmetry between donating and accepting water molecules. The existence of a single unstable mode confirmed that these structures are indeed saddle points.

Over the course of sampling transition paths, a diffusion occurs in trajectory space. Although an initial trajectory may be constructed artificially, this diffusion generates reactive trajectories with frequencies appropriate to their proper weights. After a certain period of sampling, the harvested trajectories will therefore be typical pathways that are not correlated with the initial pathway. In the sampling reported in this letter, we indeed observe diffusion away from the contrived initial trajectory. (Snapshots along the final pathway are shown in Fig. 2.) Typical proton transfer paths do not pass through the minimum-energy saddle point but rather through less symmetric, higher energy states in the transition state region. In the saddle point configuration of Fig. 1 (b), the molecules numbered 1 and 2 are equivalent. In typical paths this strict equivalence is not realized. Symmetry of the oxygen ring and symmetry of hydrogen bond angles are observed at different times along most proton transfer trajectories. As in reactive trajectories of the Stillinger-David model[7], the excess proton oscillates between molecules 1 and 2 during the transfer, while rearrangement of the oxygen

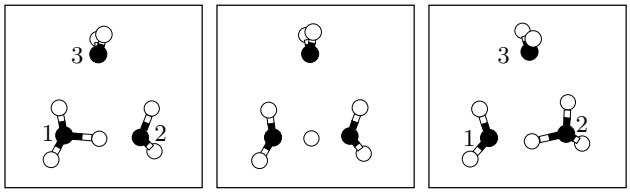

$t = 0$ $t = 20$ fs $t = 60$ fs

Figure 2. Snapshots along the final trajectory of our path sampling. In the left panel the excess proton is initially bound to molecule 1. In the middle panel, 20 fs later, the oxygen ring is symmetric and the excess proton is shared between molecules 1 and 2. At the end of this trajectory, depicted in the right panel, molecule 3 has moved across the cluster, and the proton has been transferred to molecule 2.

ring progresses nearly monotonically.

3. Transition state analysis

In analyzing transition dynamics it is instructive to classify configurations according to a probability P_B to relax into the product state. In particular, we consider a configuration to be a transition state if half of all trajectories initiated from it with random momenta relax into each stable state[13,14]. This definition allows one to search "in the dark" (i.e., without prior knowledge of the mechanism) for the collective coordinates which drive a process. We have located such a configuration along the trajectory depicted in Fig. 2. From our kinetic studies of the Stillinger-David model [7], we anticipate that $\Delta\phi = 0$ describes the transition state surface to a good approximation. For this reason we began our search at the configuration for which $\Delta\phi$ vanishes ($t = 22$ fs in this trajectory). We generated 20 trajectories from this configuration with momenta randomly selected from a microcanonical distribution. Of these trajectories only 6 relax into stable state B, i.e., $P_B \approx 0.3$. This configuration with $\Delta\phi = 0$ lies nearer the reactant's basin of attraction than the product's. Because the transferring proton oscillates between molecules 1 and 2 during the transition, its position does not seem to explain this fact. Rather, asymmetry in the strength of hydrogen bonds to the "solvating" water (molecule number 3 in Fig. 1) is a probable explanation. Characterizing these hydrogen bond strengths by their respective angles, α_i (as defined in Fig. 1), we find that the solvation of molecule 1 is stronger than that of molecule 2 in the configuration considered above. The order parameter $\Delta\alpha \equiv \alpha_1 - \alpha_2$ is plotted in Fig. 3 alongside $\Delta\phi$ for this path. The hydrogen bond angles do not become equal until later in the trajectory. Consequently, we continued our transition state search with configurations at later times. The geometries at $t = 26$ fs and $t = 30$ fs give $P_B \approx 0.4$ and $P_B \approx 0.5$, respectively. The latter configuration, a transition state, has order parameter values $\Delta\phi = 1.8°$ and $\Delta\alpha = -5°$, reflecting a compromise between oxygen ring and hydrogen bond angle symmetrization. Both of these order parameters indirectly describe the strength of hydrogen bonds from molecule 3 to the donating and accepting water molecules. Evidently, these hydrogen bonds play a central role in the transition. When the "solvating" water stabilizes donor and acceptor equally, a transition state is reached, and proton transfer may occur.

4. Proton transfer rate

The rate of an activated classical process can be computed exactly by performing averages over transition path ensembles. Straightforward calculation of these averages typically requires execution of $\sim 10^4$ shooting moves. Rate constants can be computed less expensively, however, by applying statistical transition state theory, with the transition states determined from transition path sampling. Indeed, Geissler et al. showed that the proton transfer rate in an empirical model of $(H_2O)_3H^+$ is reasonably well predicted by such a calculation, corresponding to classical RRKM theory. [3]

[3]It was reported in Ref.[7] that RRKM theory overestimates the proton transfer rate constant by a factor of ~ 15. The equation used to obtain this result, Eq. 10 of Ref.[7], however, is in error. The angular frequencies ω_i should be replaced by the corresponding frequencies ν_i, reducing the rate constant by a factor of 2π. The correct RRKM estimate differs from the path sampling result by

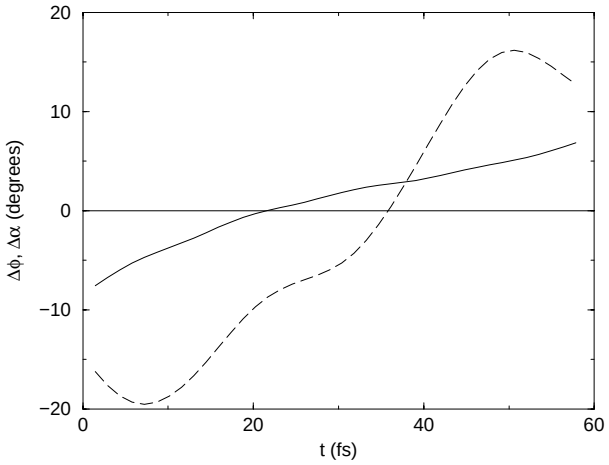

Figure 3. Order parameters $\Delta\phi$ (solid line) and $\Delta\alpha$ (dashed line) as a function of time t for the trajectory shown in Fig. 2. $\Delta\phi$ changes sign near $t = 20$ fs. $\Delta\alpha$, which characterizes peripheral hydrogen bonds, does not change sign until $t \approx 35$ fs. The transition state is located at $t \approx 30$ fs for this path.

Using vibrational properties predicted by DFT, we have computed proton transfer rate constants from both classical and quantum mechanical RRKM theory [15]. Within this theory the stable state and transition states are treated as harmonic oscillators in s and $s-1$ dimensions, respectively. Here, $s = 24$ is the number of degrees of freedom in the system. At a given energy the rate constant $k(E)$ is computed according to transition state theory. Specifically, $k(E)$ is the ratio of the number of accessible microstates at the transition state to the density of microstates in the stable region. Because the vibrational quanta of $(H_2O)_3H^+$ span a range of $1/2\,k_BT$ to $10\,k_BT$ at a temperature $T = 300$ K, classical and quantum mechanical results for $k(E)$ differ significantly at the energy studied. This discrepancy of several orders of magnitude arises primarily from zero point motion of nuclei, which effectively shifts the energy scale of the quantum mechanical system. A uniform shift in energy does not, however, influence canonical distributions. Consequently, the thermal rate constants, $k(T)$, predicted by classical and quantum mechanics agree much more closely. At $T = 300$ K quantization enhances the proton transfer rate constant by less than a factor of 2. For the lower energy transition state, quantum canonical transition state theory predicts $k = 2.3 \times 10^8\,s^{-1}$ at this temperature. For the higher energy transition state, the prediction is $k = 1.1 \times 10^8\,s^{-1}$.

The influence of quantum mechanical tunneling on proton transfer dynamics is expected to be small as well, since the unstable modes of both transition states have low associated frequencies. Modeling the potential along the reaction coordinate as a symmetric Eckart barrier, we obtain rate constant correction factors due to tunneling of 1.02 and 1.03 for the lower energy and higher energy transition states, respectively. Combining these small corrections with the transition state theory rate estimates at $T = 300$ K yields a characteristic reaction time of ~ 1 ns. This time scale is significantly shorter than that predicted by the empirical Stillinger-David force field and should be accessible experimentally.

only a factor of ~ 2.

Acknowledgments

This work was initiated with support from the National Science Foundation (grant number CHE-9508336) and completed with support from the Department of Energy through a LDRD grant administered by the Chemical Sciences Division of Lawrence Berkeley National Laboratory. C. D. was a Schrödinger Fellow of the Austrian Fonds zur Förderung der wissenschaftlichen Forschung (grants J1302-PHY and J1548-PHY) for part of this work. P. L. G. is a National Science Foundation Predoctoral Fellow and was a Berkeley Fellow for part of this work.

REFERENCES

1. C. Dellago, P. G. Bolhuis, F. S. Csajka, and D. Chandler, *J. Chem. Phys.* **108** (1998) 1964.
2. C. Dellago, P. G. Bolhuis, and D. Chandler, *J. Chem. Phys.* **108** (1998) 9236.

3. P. G. Bolhuis, C. Dellago, and D. Chandler, *Faraday Discussions* **110** (1998) 421.
4. M. Sprik, J, Hutter, and M. Parrinello *J. Chem. Phys.* **105** (1996) 1142.
5. P. M. W Gill, B. G. Johnson, J. A. Pople, *Chem. Phys. Lett.* **197** (1992) 499.
6. B. G. Johnson, P. M. W. Gill, J. A. Pople, *J. Chem. Phys.* **98** (1993) 5612.
7. P. L. Geissler, C. Dellago, and D. Chandler *Phys. Chem. Chem. Phys.* **1** (1999) 1317.
8. C. Dellago, P. G. Bolhuis, and D. Chandler, *J. Chem. Phys.* **110** (1999) 6617.
9. R. Car and M. Parrinello *Phys. Rev. Lett.* **55** (1985) 2471.
10. A. D. Becke *Phys. Rev. A* **38** (1988) 3098.
11. G. J. Martyna and M. E. Tuckerman, *J. Chem. Phys.* **110** (1999) 2810.
12. D. J. Wales, *J. Chem. Phys.* **111** (1999) 8429.
13. M. M. Klosek, B. J. Matkowsky, and Z. Schuss, *Ber. Bunsenges. Phys. Chem.* **95** (1991) 331.
14. V. Pande, A. Y. Grosberg, T. Tanaka, and E. S. Shakhnovich, *J. Chem. Phys.* **108** (1998) 334.
15. L. S. Kassel, *J. Phys. Chem.* **32** (1928) 225; O. K. Rice and H. C. Ramsperger, *J. Am. Chem. Soc.* **49** (1927) 1617; O. K. Rice and H. C. Ramsperger, *J. Am. Chem. Soc.* **50** (1927) 617; R. Marcus and O. K. Rice, *J. Phys. Colloid Chem.* **55** (1951) 894.